

Tamdy virus pathogenesis in immunocompetent and immunocompromised mouse models

Mingxue Cui^a, Hua-Chen Zhu^b, Xiurong Wang^a, Ying Cao^{c,d}, Di Liu^{c,d,e,f}, Michael J. Carr^{g,h}, Yi Guan^{b,i}, Hong Zhou^{a,j,k}, and Weifeng Shi^{a,i,l}

^aSchool of Public Health, Shandong First Medical University & Shandong Academy of Medical Sciences, Ji'nan, China; ^bState Key Laboratory of Emerging Infectious Diseases, School of Public Health, Li Ka Shing Faculty of Medicine, The University of Hong Kong, Hong Kong, China; ^cCAS Key Laboratory of Special Pathogens and Biosafety, Wuhan Institute of Virology, Center for Biosafety Mega-Science, Chinese Academy of Sciences, Wuhan, China; ^dComputational Virology Group, Center for Bacteria and Viruses Resources and Bioinformation, Wuhan Institute of Virology, Chinese Academy of Sciences, Wuhan, China; ^eInfection Management Department, People's Hospital of Xinjiang Uyghur Autonomous Region, Urumqi, China; ^fSavard Medical School, University of Chinese Academy of Sciences, Beijing, China; ^gNational Virus Reference Laboratory, University College Dublin, Dublin, Ireland; ^hInternational Collaboration Unit, Research Center for Zoonosis Control, Hokkaido University, Sapporo, Japan; ⁱShanghai Institute of Virology, Shanghai Jiao Tong University School of Medicine, Shanghai, China; ^jSchool of Clinical and Basic Medical Sciences, Shandong First Medical University & Shandong Academy of Medical Sciences, Ji'nan, China; ^kKey Laboratory of Emerging Infectious Diseases in Universities of Shandong, Shandong First Medical University & Shandong Academy of Medical Sciences, Ji'nan, China; ^lRuijin Hospital, Shanghai Jiao Tong University School of Medicine, Shanghai, China

ABSTRACT

Tamdy virus (TAMV) is one of the zoonotic tick-borne bunyaviruses that have emerged as global public health threats in recent decades. To date, however, TAMV pathogenesis remains poorly understood. In the present study, we have established different mouse infection models to enable investigation of TAMV pathogenesis. Adult BALB/c mice did not exhibit obvious clinical symptoms or signs post-TAMV infection. In contrast, adult type I interferon receptor knockout (IFNAR^{-/-}) A129 mice were found to be susceptible to high-doses of TAMV (6×10^2 and 6×10^4 FFU) and all developed severe clinical symptoms and signs, including weight loss and immobility, and reached the euthanasia criteria at 4/5-day post-infection (dpi). Viral RNA was detected in peripheral blood and different tissues (heart, liver, spleen, lung, kidney, intestine, and brain) of the high-dose infected adult A129 mice, with the highest viral loads in the liver (approximately $10^{8.3}$ copies/ μ L). Pathological examination also revealed severe liver damage in the high-dose infected A129 mice. In addition, the titres of TAMV-specific IgM and IgG antibodies increased rapidly 4–5 dpi. Analysis of cytokine and chemokine expression changes demonstrated that type I IFN may play an important role in the host defence against viral infection by enhancing IL-10 production. Gene ontology and KEGG analyses showed that liver injury may be associated with virus-induced expression of inflammatory cytokines and chemokines. Together, we have investigated TAMV pathogenesis using immunocompetent and immunocompromised mouse models, which will facilitate the development of TAMV-specific antivirals and vaccines.

ARTICLE HISTORY

Received 16 October 2024
Revised 14 February 2025
Accepted 27 April 2025

KEYWORDS


Tamdy virus; bunyavirus; mouse model; pathogenesis; IFNAR^{-/-} mice

Introduction

Bunyaviruses are negative polarity, single-stranded RNA viruses that are globally distributed. They predominantly include a diverse group of arthropod- or rodent-borne viruses that infect a wide range of vertebrate, invertebrate, and plant hosts [1]. Of note, many bunyaviruses have been previously associated with human and other mammalian febrile diseases. The most important known tick-borne bunyavirus, Crimean-Congo haemorrhagic fever virus (CCHFV), belonging to the genus *Orthobunyavirus*, family *Nairoviridae*, can cause severe haemorrhagic fever with a wide geographical distribution and case fatality rates of $\geq 30\%$ [2]. CCHFV has been listed among the

top 10 priority infectious diseases by the World Health Organization (WHO) since 2017 [3]. In addition, orthobunyaviruses, such as Dugbe virus (DUGV) [4], Nairobi sheep disease virus/Ganjam virus (NSDV/GANV) [5], and Tamdy virus (TAMV) [6], were also detected in patients with fever in Nigeria, India, and Kyrgyzstan, respectively. Moreover, several newly-identified orthobunyaviruses associated with human febrile diseases, such as Tacheng tick virus 1 (TcTV-1) [7], Songling virus (SGLV) [8], Yezo virus (YEZV) [9], Wetland virus (WELV) [10], and Xue-Cheng virus (XCV) [11], pose serious threats to animal and public health. Notably, however, no orthobunyavirus-specific antivirals or vaccines have been

CONTACT Weifeng Shi,  shiwf@ioz.ac.cn; Hong Zhou  zhouh@sdfmu.edu.cn

 Supplemental data for this article can be accessed online at <https://doi.org/10.1080/21505594.2025.2503457>

© 2025 The Author(s). Published by Informa UK Limited, trading as Taylor & Francis Group.

This is an Open Access article distributed under the terms of the Creative Commons Attribution-NonCommercial License (<http://creativecommons.org/licenses/by-nc/4.0/>), which permits unrestricted non-commercial use, distribution, and reproduction in any medium, provided the original work is properly cited. The terms on which this article has been published allow the posting of the Accepted Manuscript in a repository by the author(s) or with their consent.

developed. As a representative pathogenic orthonairovirus with a wide geographic distribution, establishment of a robust animal model of TAMV infection and accompanying pathogenesis studies are of vital importance to develop prophylactic and treatment measures against bunyaviruses.

Tamdy virus (TAMV) is a tick-borne zoonotic virus, belonging to the family *Nairoviridae*, within the genus *Orthonairovirus*. The diameter of the TAMV virion is ~90 nm [12] and the genome comprises the tripartite segments: small (S), medium (M), and large (L). These segments encode the nucleoprotein (N), glycoprotein precursor (GPC), and the RNA-dependent RNA polymerase (RdRp), respectively [13]. The TAMV (prototype strain, LEIV-1308Uz) was first isolated from *Hyalomma asiaticum asiaticum* hard-bodied ticks parasitizing sheep in the Tamdinsky district, Bukhara region, Uzbekistan in 1971 [12]. Subsequently, 52 strains of TAMV were isolated in Uzbekistan, Turkmenistan, Kyrgyzstan, Kazakhstan, Armenia, and Azerbaijan [14]. Recently, TAMV was detected for the first time in ticks collected from *Meriones tristrami* (the rodent Tristram's jird) in Turkey [15]. The first TAMV strain XJ01 from China was also isolated from *Hy. asiaticum asiaticum* infesting Bactrian camels in Xinjiang in 2018 [16].

Thus far, there have been few reports regarding TAMV infections in humans and animals. Sporadic cases associated with TAMV were reported in Kyrgyzstan in October 1973, when TAMV was isolated from the peripheral blood of a patient with fever, headache, arthralgia, and weakness [14]. It has been reported that TAMV was pathogenic in suckling and 3-week-old mice inoculated by intracerebral injection [12]. A recent study reported serological evidence of human exposure to TAMV in Northwest China [17]. Nonetheless, the precise pathogenic mechanisms of TAMV remain unclear, necessitating the development of animal infection models which are of great importance for the study of both disease pathogenesis and the development of preventative and control strategies against this tick-borne bunyavirus.

In this study, we infected BALB/c mice and type I interferon receptor knockout (IFNAR^{-/-}) mice with the TAMV strain XJ01 to assess susceptibility to infection, viral replication, tissue tropism, clinical symptoms and signs, and host responses following TAMV infection. This study provides insights into the pathogenicity of TAMV and other tick-borne viruses within the genus *Orthonairovirus* and will be invaluable for the development of therapeutic and prophylactic monoclonal antibodies and antiviral drugs.

Materials and methods

Ethics statement

The feeding and processing of the animals were subject to the guidelines of the Technical Committee on Laboratory Animal Science of the Standardization Administration of China, and the study was carried out in accordance with the approved guidelines of the Ethics Committee of Shandong First Medical University (permission no. 202004018).

Cells and virus

Human rhabdomyosarcoma (RD) cells were kindly provided by the Shandong Center for Disease Control and Prevention. RD cells were cultured in Minimum Essential Medium (MEM) (HyClone) supplemented with 10% foetal bovine serum (FBS) (Gibco) and 1% penicillin–streptomycin (Solarbio) at 37°C under 5% CO₂. The TAMV strain XJ01 (GenBank accession no. MK757580-MK757582) was isolated from *Hy. asiaticum asiaticum* ticks collected in Xinjiang, China [16]. RD cells were infected with XJ01 at a multiplicity of infection (MOI) of 0.5 for 7 days. The infected cells were harvested 7 dpi and lysed by three freeze-thaw cycles. The supernatant was collected by centrifugation at 10,000 × g for 10 min at 4°C. Viral titres were determined by focus forming unit (FFU) assay on RD cells [18]. All viruses were stored at –80°C until use.

Laboratory mice

Female BALB/c mice were purchased from Ji'nan Pengyue Experimental Animal Center (Ji'nan, China). Female IFNAR^{-/-} mice were kindly provided by Professor Gong Cheng (Tsinghua University).

All mice were housed in individually-ventilated cages under specific pathogen-free conditions. Body weight, clinical scores, and survival rates were monitored daily. Animals were scored for each parameter as follows: normal (0), ruffling (1), ruffling and slight lethargy (2), lethargy (3), laboured breathing and immobility (4). Mice showing a clinical score of 4 were considered to have reached the experimental end point and were euthanized [19].

FFU assay

RD cells were seeded at 2×10^4 cells per well in 96-well plates and incubated at 37°C under 5% CO₂. Eight hours later, the RD cells were infected with 10-fold serial dilutions of viral stocks. Twenty-four hours after infection, the media were removed, and the cells were washed three times. The cells were

then fixed with 4% Paraformaldehyde Fix Solution (Solarbio) for 10 min. The cells were washed three times with phosphate-buffered saline (PBS), permeabilized with 0.1% Triton X-100 (Sigma) for 10 min, then washed three times with PBS, and blocked with 5% bovine serum albumin (BSA; Solarbio) for 1 h at 37°C. Mouse polyclonal TAMV-positive sera [20] were diluted 1:100 with 1% BSA in PBS, incubated overnight at 4°C, and washed with PBS. The cells were stained with fluorescently tagged secondary antibody (IgG-FITC) (Solarbio) diluted 1:1,000 for 1 h at 37°C. After washing three times with PBS, the cells were incubated with DAPI (Solarbio) for 10 min at room temperature in the dark. Fluorescent plaques were observed and counted in each well using a ZEISS Axio Observer 7 fluorescence microscope to determine viral titre.

Animal infection experiments

Female BALB/c mice aged 6–8 weeks ($n = 6$ per group) were intraperitoneally injected with 6×10^2 and 6×10^4 FFU/mouse of TAMV XJ01, respectively. In addition, female IFNAR^{-/-} mice aged 6–8 weeks ($n = 5$ per group) were also intraperitoneally injected with different doses (6 , 6×10^2 , and 6×10^4 FFU/mouse) of XJ01, respectively. Each mouse was intraperitoneally injected with 40 μ L of the indicated virus dose or MEM. Uninfected control mice were administered with the culture medium and kept in a separate cage from the infected mice.

Whole blood (60–80 μ L) was collected 1, 3, 5, 7, and 14 dpi from BALB/c mice in the experimental and control groups via retro-orbital sinus bleeding, and 1, 3, and 4/5 dpi from infected IFNAR^{-/-} mice. Blood samples were used for viral load, TAMV-specific antibodies, and chemokine and cytokine detection. After euthanasia, tissues (heart, liver, spleen, lung, kidney, intestine, and brain) of the mice were harvested to perform viral load detection, pathological examination, and transcriptome sequencing. Approximately 20 μ L of whole blood or 10 mg of the tissues were used for RNA extraction, and viral load was quantified by TaqMan-based quantitative real-time reverse transcription-polymerase chain reaction (RT-qPCR). Part of each tissue was fixed with 4% paraformaldehyde for further pathological examination. The remaining tissue samples were frozen in liquid nitrogen and stored at -80°C for further use. The study adhered to the ARRIVE guidelines (<https://www.nc3rs.org.uk/arrive-guidelines>).

RNA extraction and RT-qPCR

Total RNA was extracted from whole blood/tissues (heart, liver, spleen, lung, kidney, intestine, and brain) using TRIzol reagent (TaKaRa) according to the manufacturer's protocol. Oligo-dT (18T) and random hexamer primers were employed for reverse transcription to synthesize complementary DNA (cDNA) using the Evo M-MLV RT kit (Accurate Biotechnology). Viral RNA of the L segment was quantified by TaqMan-based RT-qPCR using Pro Taq HS Premix Probe qPCR Kit (Accurate Biotechnology). The oligonucleotide primer and probe sequences for TAMV L gene are listed in Table S3. RT-qPCR was conducted on the QuantStudio 1 Real-Time PCR System (Applied Biosystems) according to the following conditions: 95°C for 10 min, followed by 40 cycles of 95°C for 15 s and 56°C for 60 s. The equation of the standard curve for TAMV L segment was $y = -3.345x + 41.69$ ($R^2 = 0.9993$). vRNA, cRNA, and mRNA of TAMV could be simultaneously detected by this assay.

Strand-specific RT-qPCR for quantitation of TAMV replication

The specific primer tagF (5'-agcatggcatagctaAATACTTCACTGTATGGGTGC-3') was employed as an RT-primer for specific synthesis of the positive strand-specific cDNAs of TAMV. The tag primer showed no sequence homology by NCBI BLAST. The reverse transcription reaction was performed using ReverTra Ace qPCR RT Kit (Toyobo) according to the manufacturer's instructions. The primer and probe sequences are listed in Table S3. cRNA and mRNA of TAMV could be simultaneously detected by this strand-specific RT-qPCR assay.

ELISA detection of anti-TAMV antibody

Blood samples from mice in the different experimental groups were centrifuged for 10 min at 3 000 rpm to separate the plasma used for anti-TAMV antibody detection. In-house recombinant nucleoprotein of TAMV was used as the coating antigen to evaluate viral-specific antibodies in the plasma in the ELISA assay, as described previously [20]. Briefly, recombinant nucleoprotein diluted to 0.25 $\mu\text{g/mL}$ with carbonate-bicarbonate buffer (pH 9.6) was used to coat 96-well plate and incubated at 4°C overnight. Plates were washed three times with washing buffer (Lianke), which were then blocked for 90 min at 37°C using 1% BSA (Solarbio), followed by washing. Plasma samples diluted 1:400 by 0.1% BSA in washing buffer were

added to the plates (100 μ L per well) and incubated for 1 h at 37°C. After washing three times, 100 μ L goat anti-mouse IgM-horseradish peroxidase (HRP) or goat anti-mouse IgG-HRP (1:5,000 dilution) (Solarbio) was added for 1 h at 37°C. After washing, 3,3',5,5'-tetramethylbenzidine (TMB) substrate (Lianke) was added and the reaction was terminated by adding 1 M sulphuric acid (Lianke) after 15 min incubation in the dark at 37°C. The absorbance at 450 nm of each well was recorded using a microplate reader (BioTek ELx808).

Chemokine and cytokine analysis

Female BALB/c and IFNAR^{-/-} mice (6–8 weeks old) were challenged with different doses of TAMV or MEM medium by intraperitoneal injection. Peripheral blood was collected via the retro-orbital sinus. After RNA extraction and reverse transcription, the mRNA expression of chemokine and cytokines was determined by RT-qPCR using SYBR Green Premix Pro Taq HS qPCR Kit (Accurate Biology). Relative mRNA expression was calculated by the $2^{-\Delta\Delta C_t}$ method. The primers used for RT-qPCR are provided in Table S3.

Histological examination

Tissue samples of heart, liver, spleen, lung, kidney, intestine, and brain of the experimental groups of IFNAR^{-/-} mice infected with TAMV were separated at 4/5 dpi. Tissues of the control group were separated at 5 dpi. Samples were fixed in 4% paraformaldehyde and embedded in paraffin according to previously described procedures [21]. Paraffin-embedded tissue sections (4 μ m) were stained with haematoxylin and eosin (H&E) for histological examination. Embedding, sectioning, H&E staining, and analysis were performed by Wuhan Servicebio Technology.

Transcriptome sequencing

Total RNA was extracted from liver tissues of the control group and the 6×10^4 FFU group of female IFNAR^{-/-} mice. RNA samples with high integrity were used for RNA-seq library preparation. After the library was quantified, sequencing was performed on an Illumina NovaSeq 6000 sequencing platform with 150 bp paired-end reads (performed by the Novogene Bioinformatics Technology Company). FeatureCounts v1.5.0-p3 was used to count the reads numbers mapped to each gene, and then Fragments Per Kilobase of transcript per Million mapped reads (FPKM) for each gene was calculated based on the length of the gene and reads count

mapped to this gene. Differential expression analysis of two groups was performed using the DESeq2 R package (1.20.0). Differentially expressed transcripts were screened based on the criteria of \log_2 (Fold Change) >1 and $p_{\text{adj}} < 0.05$. The GO enrichment analysis of differentially-expressed genes was implemented by the clusterProfiler R package (3.8.1).

Statistical analysis

Statistical analyses and graphics were performed using GraphPad prism 8. The survival curves were analysed using log-rank (Mantel–Cox test) analysis. Statistical differences between different groups were analysed using one-way analysis of variance (ANOVA). Independent samples t-test was used to analyse the differences of viral load between the 6×10^2 FFU and 6×10^4 FFU groups of IFNAR^{-/-} mice. If the data did not conform to a normal distribution, then a non-parametric test was used. If the data were normally distributed but the variances were not equal, the Brown-Forsythe and Welch ANOVA with Dunnett multiple comparison tests were used. All data were presented as the means \pm standard deviation (SD).

Results

Clinical symptoms and signs of TAMV infected BALB/c and IFNAR^{-/-} mice

Female BALB/c mice aged 6–8 weeks were challenged through the intraperitoneal (i.p.) route with 6×10^2 FFU/mouse and 6×10^4 FFU/mouse TAMV, respectively (Figure 1(a)). Compared with the control group, the animal weight did not significantly change in the 6×10^2 FFU group but decreased in the 6×10^4 FFU group (Figure 2(a)). Meanwhile, the mice in the 6×10^2 FFU group did not exhibit any discernible clinical manifestations, and the mice in the 6×10^4 FFU group only presented ruffling at 2–5 days post-infection (dpi) with the maximum clinical score of 1 (Table S1). All BALB/c mice survived during the challenge experiment.

Female IFNAR^{-/-} mice aged 6–8 weeks were also challenged through the i.p. route with different doses (6 , 6×10^2 , and 6×10^4 FFU/mouse) of TAMV (Figure 1(b)). The mice in the 6×10^2 FFU and 6×10^4 FFU groups showed significant weight losses compared to those animals in the control group, whereas the mice in the 6 FFU group showed no significant changes in body weight (Figure 2(b)). Mice in the 6×10^2 FFU and 6×10^4 FFU groups presented ruffling 3 dpi and subsequently progressed to immobility 4/5 dpi with the highest clinical scores (Table S2). In contrast, the 6 FFU

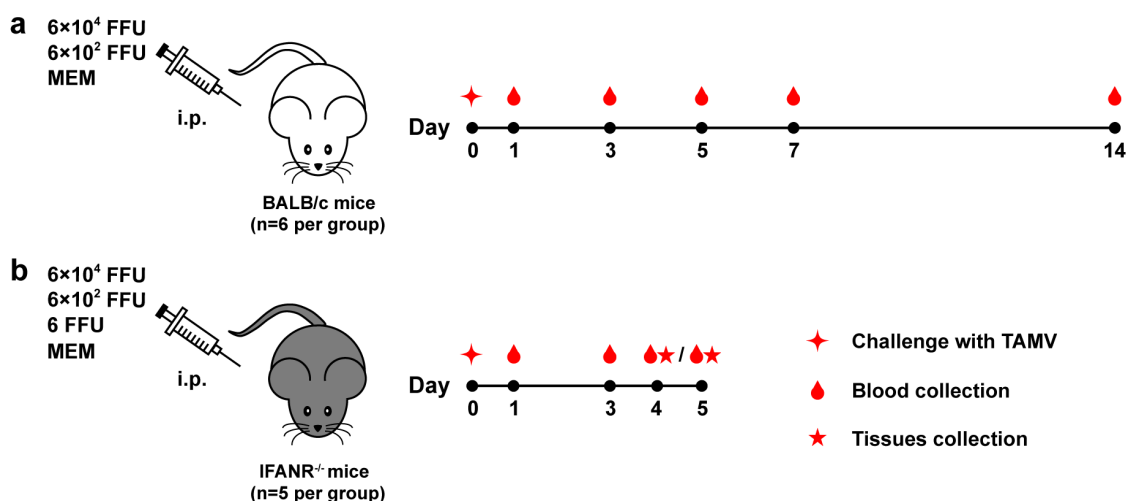


Figure 1. Schematic diagram of the experimental design.

(a) BALB/c mice and (b) IFNAR^{-/-} mice infected with different doses of TAMV by intraperitoneal injection.

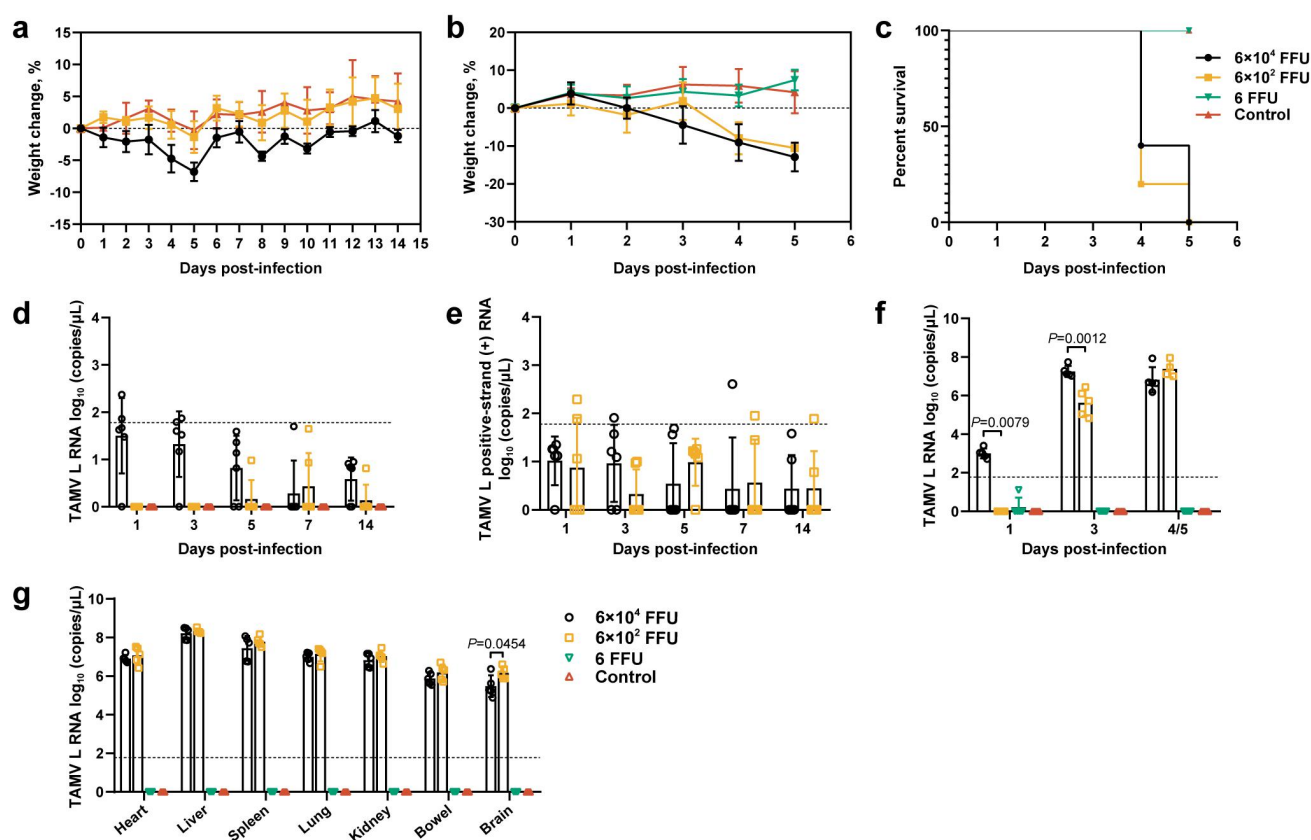


Figure 2. Body weight changes, survival curves, and viral RNA in TAMV-infected BALB/c mice and IFNAR^{-/-} mice.

(a) Body weight changes in different groups of BALB/c mice after challenge with TAMV. (b) Body weight changes and (c) survival curves in different groups of IFNAR^{-/-} mice after challenge with TAMV. (d) Blood viral loads detected by RT-qPCR and (e) viral replication assessed by strand-specific RT-qPCR in different groups of BALB/c mice after challenge with TAMV. Viral loads in (f) blood and (g) seven tissues of IFNAR^{-/-} mice infected with different doses of TAMV. Data were expressed as means \pm SD. The dotted line represents the limit of detection for the RT-qPCR assay.

group did not show any clinical manifestations (Table S2). For the two high-dose groups (6×10^2 and 6×10^4 FFU), all the mice reached the

euthanasia criteria at 4/5 dpi; however, in the low-dose group (6 FFU), all the mice survived out to 5 dpi (Figure 2(c)).

TAMV replication in infected BALB/c and IFNAR^{-/-} mice

Whole blood from female BALB/c mice was collected 1, 3, 5, 7, and 14 dpi, respectively. No viral loads were observed in the 6×10^2 FFU infection group and only low viral loads (approximately $10^{0.81}$ – $10^{2.37}$ copies/ μ L) of TAMV were detectable in the whole blood of BALB/c mice in the 6×10^4 FFU infection group at all time points post-infection (Figure 2(d)). Two-step, strand-specific TaqMan-based RT-qPCR was performed to detect the TAMV positive-stranded RNA in the blood, which is indicative of viral replication. Again, a low viral load (approximately $10^{0.78}$ – $10^{2.61}$ copies/ μ L) of positive-stranded TAMV RNA was detected by strand-specific RT-qPCR in blood of the 6×10^2 FFU and 6×10^4 FFU groups at all time points post-infection (Figure 2(e)). These results demonstrated that TAMV might have limited infectivity in BALB/c mice.

Female IFNAR^{-/-} mice were euthanized 4/5 dpi, with whole blood collected 1, 3, and 4/5 dpi, respectively. In the 6 FFU and control groups, no viral RNA was detectable from the whole blood (Figure 2(f)). In the 6×10^4 FFU group, a low viral load (approximately 10^3 copies/ μ L) of TAMV was detected 1 dpi, which reached a peak (approximately $10^{7.3}$ copies/ μ L) 3 dpi, and then decreased slightly (approximately $10^{6.8}$ copies/ μ L) 4/5 dpi (Figure 2(f)). In the 6×10^2 FFU group, TAMV was not detected 1 dpi, however, was detected (approximately $10^{5.6}$ copies/ μ L) at the 3 dpi timepoint. The viral load gradually increased and reached a peak (approximately $10^{7.4}$ copies/ μ L) 4/5 dpi (Figure 2(f)).

For female IFNAR^{-/-} mice, all the mice in the 6×10^2 FFU and 6×10^4 FFU groups were euthanized 4/5 dpi. At the same time, all the mice in the 6 FFU and control groups were also euthanized 5 dpi although they had not met the euthanasia criteria. TAMV was not detected in all the tissues that were tested (heart, liver, spleen, lung, kidney, intestine, and brain) of the mice in the 6 FFU and control groups (Figure 2(g)). Conversely, TAMV was detected in all the tissues of the 6×10^2 FFU and 6×10^4 FFU groups (Figure 2(g)). Of note, among all the studied tissues, the viral load in the liver was the highest (approximately $10^{8.3}$ copies/ μ L) (Figure 2(g)).

Pathological examination of the TAMV infected IFNAR^{-/-} mice

The tissues (heart, liver, spleen, lung, kidney, intestine, and brain) of the IFNAR^{-/-} mice in the experimental

and control groups were stained with H&E to assess potential pathological changes. H&E staining of the liver tissues of the IFNAR^{-/-} mice in the 6×10^2 FFU and 6×10^4 FFU groups showed large areas of cellular necrosis, nuclear fragmentation and/or lysis accompanied by scattered lymphocytic infiltration (Figure 3). In addition, H&E staining of the lung tissues in the 6×10^2 FFU and 6×10^4 FFU groups showed that the alveolar wall was slightly thickened with scattered granulocytic infiltration (Figure 3). No obvious pathological abnormalities were observed in the other tissues (heart, spleen, kidney, intestine, and brain) in the 6×10^2 FFU and 6×10^4 FFU experimental groups (Figure 3). No obvious pathological abnormalities were observed in all tissues from the 6 FFU and control groups (Figure 3).

Antibody responses in TAMV-infected BALB/c and IFNAR^{-/-} mice

Whole blood was collected from the orbital sinuses of the mice, and serum was obtained by centrifugation. Anti-TAMV IgM and IgG antibodies were detected by indirect enzyme-linked immunosorbent assay (ELISA). The IgM antibody titres of the BALB/c mice in the 6×10^2 FFU and 6×10^4 FFU groups showed a slight increase at 1 dpi, and no significant differences were determined during the remaining experimental time course compared to the control group (Figure 4(a)). In the BALB/c mice in the 6×10^4 FFU group, IgG antibody began to increase 7 dpi, and increased significantly 14 dpi (Figure 4(b)). In the BALB/c mice of the 6×10^2 FFU group, IgG antibody also increased 14 dpi compared to the control group (Figure 4(b)). In contrast, the IFNAR^{-/-} mice in the 6×10^2 FFU and 6×10^4 FFU groups showed simultaneous elevation of IgG and IgM antibodies 4–5 dpi, whereas both antibodies in the 6 FFU group did not increase compared to the control group (Figure 4(c,d)).

Cytokine expression levels in TAMV-infected BALB/c and IFNAR^{-/-} mice

The mRNA quantities of cytokines and chemokines in peripheral blood were assayed by RT-qPCR. For wild-type (WT) BALB/c mice, the levels of pro-inflammatory cytokines and chemokines (MIP-1 α , MIP-1 β , TNF- α , IFN- γ , and RANTES) and anti-inflammatory cytokines (IL-10) in the TAMV-infected group were significantly greater than the control group (Figure 5(a–f)). However, levels of other pro-inflammatory cytokines, such as IL-6 and IL-1 β , were not significantly higher compared to the control group (Figure 5(g,h)).

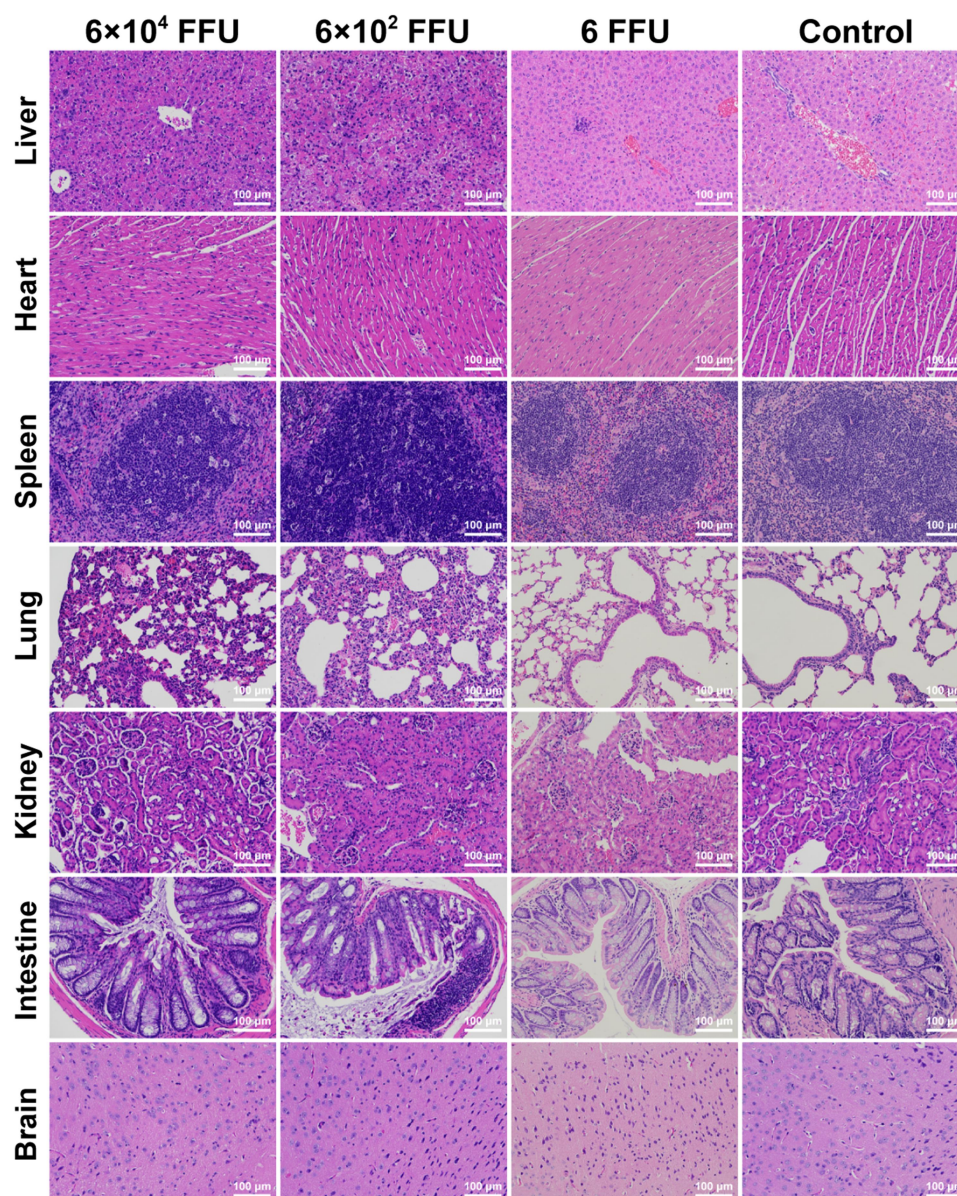


Figure 3. Histopathological changes in different tissues of $IFNAR^{-/-}$ mice infected with different doses of TAMV.

The investigated tissues included the liver, heart, spleen, lung, kidney, intestine, and brain. Histopathological analysis was performed by H&E staining. Scale bar: 100 μ m.

For $IFNAR^{-/-}$ mice, the levels of cytokines and chemokines in the infected group were not entirely consistent with those in the BALB/c mice. Specifically, the levels of pro-inflammatory cytokines and chemokines (MIP-1 α , MIP-1 β , TNF- α , and IL-1 β) were higher in the high-dose groups (6×10^2 and 6×10^4 FFU) compared with the control group (Figure 5(a–c,h)). However, IFN- γ was downregulated after TAMV infection (Figure 5(d)). RANTES was first upregulated and then downregulated (Figure 5(e)). In addition, the levels of IL-10 and IL-6 in the high-dose groups were not significantly higher than those in the control group (Figure 5(f,g)).

Transcriptomic analysis of liver tissue in TAMV-infected $IFNAR^{-/-}$ mice

RNA sequencing analysis (RNA-seq) was performed to explore differential gene expression in the liver tissues of the $IFNAR^{-/-}$ mice between the control group and the 6×10^4 FFU group. The heatmaps showed similar gene expression patterns within the same group, with distinct differences observed between groups (Figure 6(a)). Volcano plot revealed that 6,048 genes were differentially expressed between the two groups, including 3,090 upregulated genes and 2,958 downregulated genes (the 6×10^4 FFU group versus the control

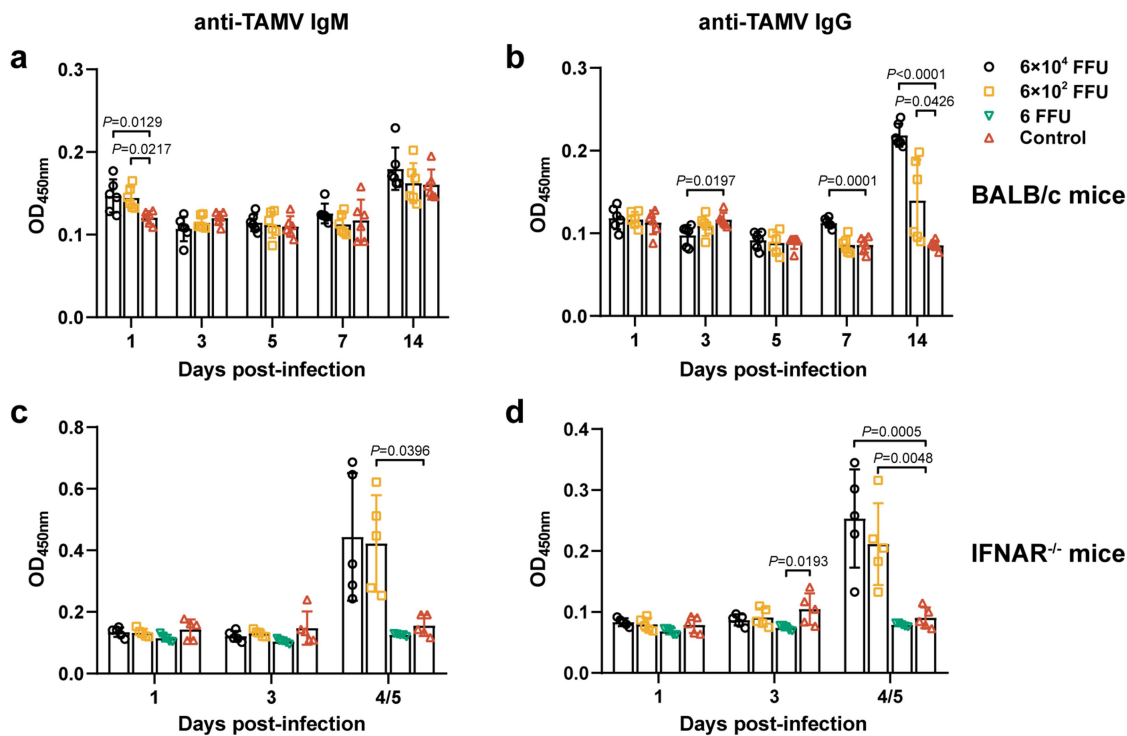


Figure 4. Anti-TAMV serum antibody responses.

IgM and IgG antibody responses in (a-b) BALB/c mice and (c-d) IFNAR^{-/-} mice infected with different doses of TAMV. Data were expressed as means \pm SD.

group) (Figure 6b)). Among them, Ubiquitin D (UBD), Interferon Induced Protein With Tetratricopeptide Repeats 2 (IFIT2), Interferon Induced Protein With Tetratricopeptide Repeats 1 (IFIT1), Radical S-Adenosyl Methionine Domain-Containing Protein 2 (RSAD2), and Lymphocyte antigen 6D (LY6D) were the top five upregulated genes, whereas Coenzyme Q8A (COQ8A), Indolethylamine N-Methyltransferase (INMT), Transmembrane 7 Superfamily Member 2 (TM7SF2), Aquaporin 8 (AQP8), and TLC Domain Containing 2 (TLCD2) were the top five downregulated genes (Figure 6b)).

We then performed Gene Ontology (GO) and Kyoto Encyclopedia of Genes and Genomes (KEGG) enrichment analyses of the significantly upregulated differentially-expressed genes (DEGs). We analysed the top 30 GO terms with the most significant differences from the GO enrichment analysis (Figure 6c)). The biological processes (BP) associated with these upregulated DEGs were significantly enriched for DNA replication and regulation of cell death. In the cell component (CC) category, the upregulated DEGs were mainly enriched in the chromosomal region and chromosome categories. The most significantly enriched molecular functions of the upregulated DEGs were cytokine

receptor binding and G-protein-coupled receptor activity. We also analysed the most significant 20 KEGG pathways (Figure 6d)) and found that DEGs were significantly enriched in cytokine-cytokine receptor interaction, viral protein interaction with cytokine and cytokine receptor, and the chemokine signalling pathway.

Discussion

As a neglected zoonotic pathogen, TAMV may also have important effects on regional public and animal health, particularly in mid-, southern, and western Asia, where the major host vector of TAMV - *Hy. asiaticum asiaticum* - is endemic. Understanding the pathogenicity of TAMV is important for the development of antivirals and prophylactic and therapeutic countermeasures. To this end, establishment of a robust animal model of TAMV infection is a major prerequisite to drug discovery.

IFNAR^{-/-} mice are a useful animal model to investigate the pathogenesis of tick-borne bunyaviruses, and it has been reported that some tick-borne bunyaviruses, including SFTSV [22,23], Issyk-Kul virus [24], soft tick bunyavirus [24], Tofla virus [25],

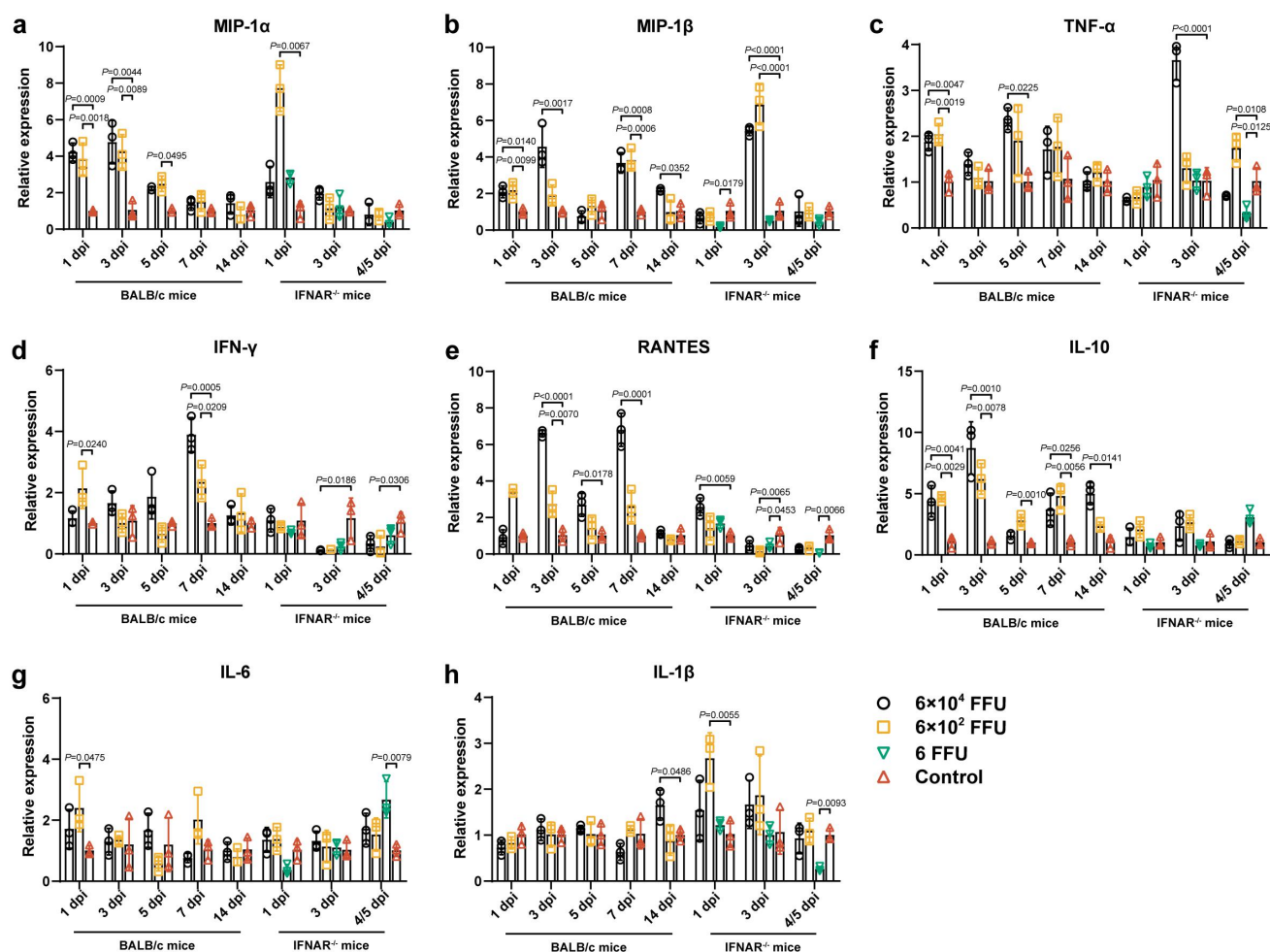


Figure 5. Cytokine and chemokine mRNA transcription profiles in the peripheral blood of BALB/c and IFNAR^{-/-} mice after TAMV challenge.

The mRNA levels of (a) MIP-1α, (b) MIP-1β, (c) TNF-α, (d) IFN-γ, (e) RANTES, (f) IL-10, (g) IL-6, and (h) IL-1β in the blood of BALB/c and IFNAR^{-/-} mice were quantified by RT-qPCR at different time points after TAMV infection. All genes were normalized to β-actin by the 2^{-ΔΔCt} method. Data were expressed as means ± SD (*n* = 3).

YEZV [26], as well as CCHFV [27,28], do not manifest clinical symptoms or signs in wild-type mice, however, induce lethal infection in IFNAR^{-/-} mice. In the present study, after challenge with high-doses (6×10^2 and 6×10^4 FFU) of TAMV, immunocompetent wild-type mice did not show obvious clinical manifestations, whereas IFNAR^{-/-} mice developed severe disease and all animals reached euthanasia criteria 4–5 dpi. BALB/c mice infected with TAMV via the i.p. route did not show severe symptoms caused by haemorrhagic fever viruses in IFN-deficient mice (i.e. lack of responsiveness to stimuli, significant hypoactivity and/or weight loss, or neurologic abnormalities) [29]. These findings suggest the potential for severe and even fatal outcomes following TAMV infection in both immunodeficient and immunosuppressed individuals, and, also, that IFN may mediate the antiviral response against TAMV infection.

At the same time, all IFNAR^{-/-} mice infected with high-dose TAMV showed obvious clinical symptoms, such as ruffling, immobility, and significant weight loss, and reached euthanasia criteria 4–5 dpi. High viral loads of TAMV were detected in the peripheral blood and tissues in the high-dose infected mice, with the liver exhibiting the highest viral load. Apart from the liver, where severe damage was observed, no obvious pathological abnormalities were found in other tissues. Therefore, adult female IFNAR^{-/-} mice may be readily susceptible to TAMV infection with high doses and result in fatal outcomes, with the liver being a more susceptible organ to TAMV infection.

Typically, in the innate immune system, the interactions between pathogen-associated molecular patterns and host pattern recognition receptors induce the production of pro-inflammatory cytokines to elicit antiviral responses [30]. However, the secretion of anti-

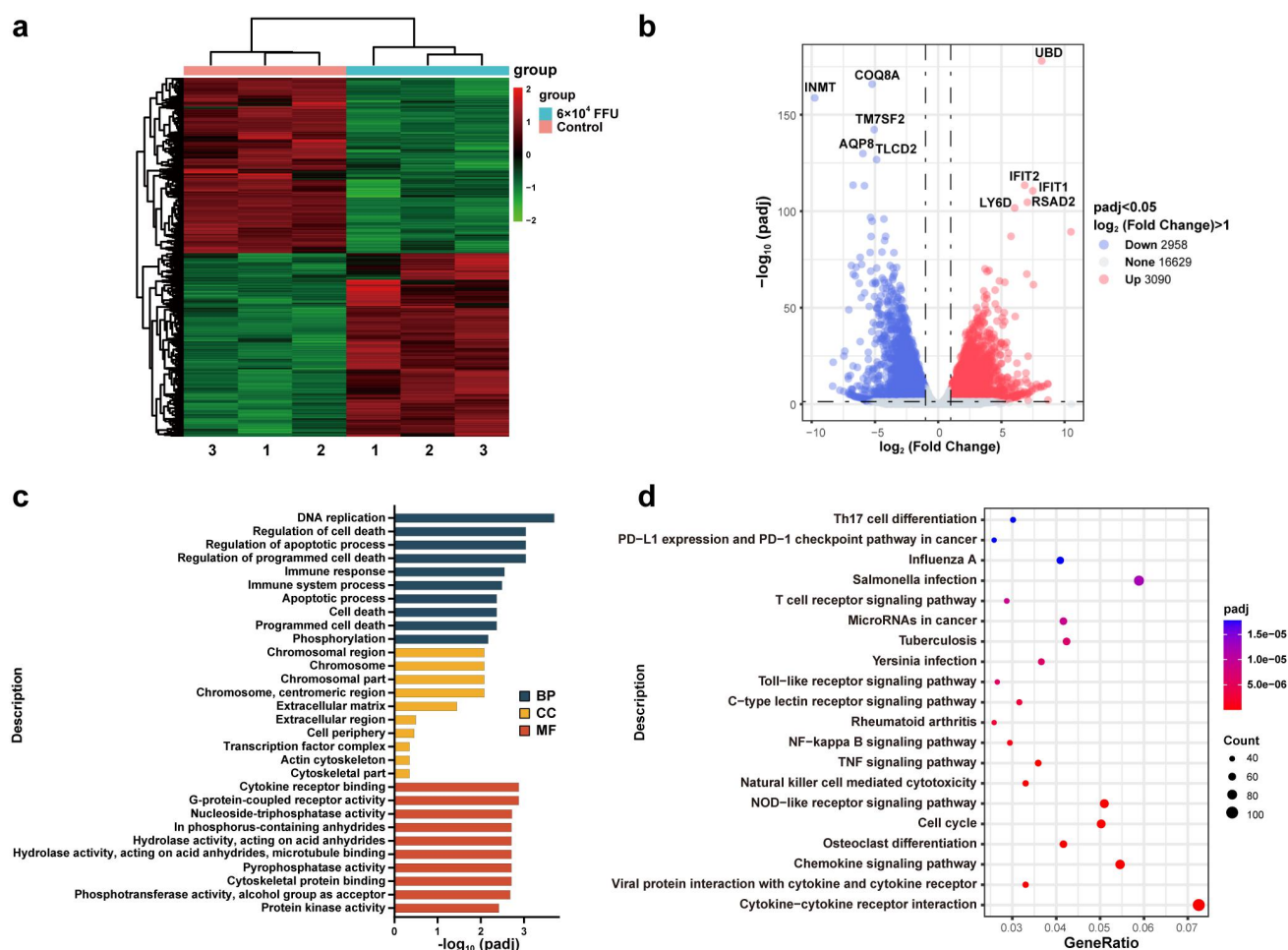


Figure 6. Transcriptomic analysis of IFNAR^{-/-} mice liver by RNA sequencing (RNA-Seq) after TAMV challenge.

(a) Heatmap and (b) volcano plot of differentially expressed genes. (c) GO and (d) KEGG enrichment analysis of the upregulated genes. BP, Biological Process; CC, Cellular Component; MF, Molecular Function; GO, gene ontology; KEGG, Kyoto Encyclopedia of Genes and Genomes.

inflammatory cytokines can control excessive inflammatory responses [31]. High-dose infection of TAMV-infected IFNAR^{-/-} mice showed significant differences in the expression levels of cytokines and chemokines compared with wild-type mice. Post-TAMV infection, pro-inflammatory cytokines and chemokines (MIP-1 α , MIP-1 β , TNF- α , IFN- γ , and RANTES) and anti-inflammatory cytokines (IL-10) were upregulated in BALB/c mice. However, no significant changes of IL-10 levels were observed in the IFNAR^{-/-} mice. A previous study showed that IL-10, an anti-inflammatory cytokine, targets both innate and adaptive immune responses and exerts immunosuppressive functions to reduce tissue damage caused by excessive and uncontrolled inflammatory effector responses [32]. Type I IFNs are known to induce IL-10 [33]. Thus, we hypothesize that the reduction in IL-10 production due to the absence of IFNAR signalling might have reduced the inhibition of excessive production of pro-inflammatory cytokines, eventually resulting in

a cytokine storm that aggravates liver damage and causes the deaths of TAMV-infected IFNAR^{-/-} mice. This hypothesis is also supported by a previous study in which IFNAR^{-/-} mice presented impaired IL-10 production and developed lung damage, while they showed an improved survival rate and reduced lung damage after the addition of exogenous IL-10 [34]. Moreover, compared with those in BALB/c mice, the significant upregulation of pro-inflammatory cytokines (MIP-1 α , MIP-1 β , and TNF- α) following high-dose TAMV infection in IFNAR^{-/-} mice lends further support to this hypothesis. The above results reveal that type I IFNs may play important roles in the host defence against viral infection by increasing IL-10 production to suppress excessive production of pro-inflammatory cytokines.

To further elucidate the molecular mechanism of TAMV-induced liver damage, we performed a transcriptome analysis. UBD, the most significantly upregulated gene, is a ubiquitin-like protein whose

expression can be elicited by both IFN- γ and TNF- α [35]. Within the host cell, viral RNA triggers the activation of the RIG-I signalling pathway, leading to the production of IFN-I. However, IFN-I plays a dual role in modulating antiviral immunity and/or immunopathology during viral infections. The exaggerated IFN-I responses can cause severe tissue damage [36]. In this study, large amounts of IFN-I are produced by viral infection in IFNAR^{-/-} mice. UBD could induce proteasomal degradation and function as a negative regulator of IFN-I production [37], thereby attenuating excessive IFN-I-mediated tissue damage. Remarkably, the other four most upregulated genes were also related to antiviral immunity. IFIT1 and IFIT2 are members of the IFIT family. IFITs are potent inhibitors of viral RNA translation [38] and have been shown to inhibit many viruses, including Sendai virus, vesicular stomatitis virus, West Nile virus (WNV), and hepatitis C virus (HCV) [39]. RSAD2, a member of the radical S-adenosyl-L-methionine (SAM) superfamily, showed antiviral activity against a range of RNA viruses, including dengue virus, WNV, HCV, influenza A virus, Japanese encephalitis virus, and yellow fever virus [40,41]. LY6D is a member of the LY6 family, and the LY6 superfamily has been considered to play an important role in innate immunity in mammals [42]. GO and KEGG enrichment analyses showed that these upregulated genes were mainly enriched in cytokine receptor binding, cytokine-cytokine receptor interaction, and chemokine signalling pathway. Therefore, transcriptome analysis showed that antiviral immunity-related genes were significantly upregulated in the liver of IFNAR^{-/-} mice infected with TAMV. However, GO and KEGG enrichment analysis suggested that the liver injury may be associated with virus-induced expression of inflammatory cytokines and chemokines.

In summary, we revealed the potential heterogeneous pathogenesis of TAMV in BALB/c and IFNAR^{-/-} murine models, and found that high-dose TAMV infection in IFNAR^{-/-} mice could lead to fulminant and fatal disease, without obvious clinical manifestations observed in BALB/c mice. High viral loads of TAMV were detected in several tissues and blood of IFNAR^{-/-} mice, causing severe liver damage. These findings highlight the potential lethal threat of TAMV to immunocompromised populations, the need for surveillance of TAMV in humans (particularly occupational populations with animal husbandry) and farmed livestock. These infection models will be useful for the development of prophylactic and therapeutic countermeasures against this neglected tick-borne pathogen.

Disclosure statement

No potential conflict of interest was reported by the author(s).

Funding

This study was supported by grants from the National Natural Science Foundation of China (NSFC) for Distinguished Young Scholars [32325003 to WS], National Natural Science Foundation of China [82202516], Taishan Scholars Programme of Shandong Province [tsqn202306264 to HZ], and Joint Innovation Team for Clinical & Basic Research [202407].

Author contributions

Conceptualization: HZ and WS; Methodology: MC and XW; Formal analysis: MC; Visualization: MC; Resources: HCZ, YC, DL, and YG; Writing-original draft: MC; Writing-review and editing: MJC, HZ, and WS; Funding acquisition: HZ and WS. All the authors have read and approved the manuscript.

Data availability statement

The authors confirm that the study data is available within the article and supplemental materials and is also openly available in Figshare at <https://doi.org/10.6084/m9.figshare.28416212>. Transcriptomic sequencing data supporting the findings of this study have been deposited to the NCBI Sequence Read Archive (SRA) database under BioProject accession number PRJNA1171487 (SRA accession numbers: SRR30947216-SRR30947221).

ORCID

Di Liu  <http://orcid.org/0000-0003-3693-2726>
Weifeng Shi  <http://orcid.org/0000-0002-8717-2942>

References

- [1] Malet H, Williams HM, Cusack S, et al. The mechanism of genome replication and transcription in bunyaviruses. *PLOS Pathog.* 2023;19(1):e1011060. doi: [10.1371/journal.ppat.1011060](https://doi.org/10.1371/journal.ppat.1011060)
- [2] Hawman DW, Feldmann H. Crimean-Congo haemorrhagic fever virus. *Nat Rev Microbiol.* 2023;21(7):463–477. doi: [10.1038/s41579-023-00871-9](https://doi.org/10.1038/s41579-023-00871-9)
- [3] Mehand MS, Al-Shorbaji F, Millett P, et al. The WHO R&D blueprint: 2018 review of emerging infectious diseases requiring urgent research and development efforts. *Antiviral Res.* 2018;159:63–67. doi: [10.1016/j.antiviral.2018.09.009](https://doi.org/10.1016/j.antiviral.2018.09.009)
- [4] David-West TS. Dugbe virus: a new tick-borne arbovirus from Nigeria. *Trans R Soc Trop Med Hyg.* 1973;67(4):438. doi: [10.1016/0035-9203\(73\)90062-x](https://doi.org/10.1016/0035-9203(73)90062-x)
- [5] Sudeep AB, Jodi RS, Mishra A, et al. Ganjam virus. *Indian J Med Res.* 2009;130(5):514–519.

- [6] L'vov DS, Gromashevskii VL, Skvortsova TM, et al. Isolation of tamdy virus (Bunyaviridae) pathogenic for man from natural sources in central Asia, Kazakhstan and Transcaucasia. *Vopr Virusol.* 1984;29(4):487–490.
- [7] Liu XF, Zhang X, Wang ZD, et al. A tentative tamdy orthonairovirus related to febrile illness in Northwestern China. *Clin Infect Dis.* 2020;70(10):2155–2160. doi: [10.1093/cid/ciz602](https://doi.org/10.1093/cid/ciz602)
- [8] Ma J, Lv X-L, Zhang X, et al. Identification of a new orthonairovirus associated with human febrile illness in China. *Nat Med.* 2021;27(3):434–439. doi: [10.1038/s41591-020-01228-y](https://doi.org/10.1038/s41591-020-01228-y)
- [9] Kodama F, Yamaguchi H, Park E, et al. A novel nairovirus associated with acute febrile illness in Hokkaido, Japan. *Nat Commun.* 2021;12(1):5539. doi: [10.1038/s41467-021-25857-0](https://doi.org/10.1038/s41467-021-25857-0)
- [10] Zhang X-A, Ma Y-D, Zhang Y-F, et al. A new orthonairovirus associated with human febrile illness. *N Engl J Med.* 2024;391(9):821–831. doi: [10.1056/NEJMoa2313722](https://doi.org/10.1056/NEJMoa2313722)
- [11] Zhang M-Z, Bian C, Ye R-Z, et al. Human infection with a novel tickborne orthonairovirus species in China. *N Engl J Med.* 2025;392(2):200–202. doi: [10.1056/NEJMc2410853](https://doi.org/10.1056/NEJMc2410853)
- [12] Lvov DK, Sidorova GA, Gromashevsky VL, et al. Virus “tamdy”—a new arbovirus, isolated in the Uzbee S.S. R. and Turkmen S.S.R. from ticks *hyalomma asiaticum asiaticum* schulee et schlottke, 1929, and *hyalomma plumbeum plumbeum* panzer, 1796. *Arch Virol.* 1976;51(1–2):15–21. doi: [10.1007/BF01317830](https://doi.org/10.1007/BF01317830)
- [13] Kuhn JH, Alkhovsky SV, Aysic-Zupanc T, et al. ICTV virus taxonomy profile: nairoviridae 2024. *J Gen Virol.* 2024;105(4):001974. doi: [10.1099/jgv.0.001974](https://doi.org/10.1099/jgv.0.001974)
- [14] Lvov DK, Shchelkanov MY, Alkhovsky SV, et al. Zoonotic viruses of Northern Eurasia: taxonomy and ecology. New York: Academic Press; 2015.
- [15] Brinkmann A, Dincer E, Polat C, et al. A metagenomic survey identifies tamdy orthonairovirus as well as divergent phlebo-, rhabdo-, chu- and flavi-like viruses in Anatolia, Turkey. *Ticks Tick Borne Dis.* 2018;9(5):1173–1183. doi: [10.1016/j.ttbdis.2018.04.017](https://doi.org/10.1016/j.ttbdis.2018.04.017)
- [16] Zhou H, Ma Z, Hu T, et al. Tamdy virus in ixodid ticks infesting bactrian camels, Xinjiang, China, 2018. *Emerg Infect Dis.* 2019;25(11):2136–2138. doi: [10.3201/eid2511.190512](https://doi.org/10.3201/eid2511.190512)
- [17] Moming A, Shen S, Fang Y, et al. Evidence of human exposure to tamdy virus, Northwest China. *Emerg Infect Dis.* 2021;27(12):3166–3170. doi: [10.3201/eid2712.203532](https://doi.org/10.3201/eid2712.203532)
- [18] Anne FP, Iwona B-G, Elizabeth BK, et al. Quantitation of flaviviruses by fluorescent focus assay. *J Virol Methods.* 2006. doi: [10.1016/j.jviromet.2006.01.003](https://doi.org/10.1016/j.jviromet.2006.01.003)
- [19] Pavel STI, Yetiskin H, Kalkan A, et al. Evaluation of the cell culture based and the mouse brain derived inactivated vaccines against Crimean-Congo hemorrhagic fever virus in transiently immune-suppressed (IS) mouse model. *PLOS Negl Trop Dis.* 2020;14(11):e0008834. doi: [10.1371/journal.pntd.0008834](https://doi.org/10.1371/journal.pntd.0008834)
- [20] Cui M, Bi Y, Guo M, et al. Serological evidence of bactrian camel infection with tamdy virus, Xinjiang, China. *Vector-Borne Zoonotic Dis.* 2024;24(12):842–845. doi: [10.1089/vbz.2024.0019](https://doi.org/10.1089/vbz.2024.0019)
- [21] Li H, Zhang LK, Li SF, et al. Calcium channel blockers reduce severe fever with thrombocytopenia syndrome virus (SFTSV) related fatality. *Cell Res.* 2019;29(9):739–753. doi: [10.1038/s41422-019-0214-z](https://doi.org/10.1038/s41422-019-0214-z)
- [22] Liu Y, Wu B, Paessler S, et al. The pathogenesis of severe fever with thrombocytopenia syndrome virus infection in alpha/beta interferon knockout mice: insights into the pathologic mechanisms of a new viral hemorrhagic fever. *J Virol.* 2014;88(3):1781–1786. doi: [10.1128/JVI.02277-13](https://doi.org/10.1128/JVI.02277-13)
- [23] Park SC, Park JY, Choi JY, et al. Pathogenicity of severe fever with thrombocytopenia syndrome virus in mice regulated in type I interferon signaling: severe fever with thrombocytopenia and type I interferon. *Lab Anim Res.* 2020;36(1):38. doi: [10.1186/s42826-020-00070-0](https://doi.org/10.1186/s42826-020-00070-0)
- [24] Sugimoto S, Suda Y, Nagata N, et al. Characterization of ketterah orthonairovirus and evaluation of therapeutic candidates against ketterah orthonairovirus infectious disease. *Ticks Tick Borne Dis.* 2022;13(1):101834. doi: [10.1016/j.ttbdis.2021.101834](https://doi.org/10.1016/j.ttbdis.2021.101834)
- [25] Shimada S, Aoki K, Nabeshima T, et al. Tofla virus: a newly identified nairovirus of the Crimean-Congo hemorrhagic fever group isolated from ticks in Japan. *Sci Rep.* 2016;6(1):20213. doi: [10.1038/srep20213](https://doi.org/10.1038/srep20213)
- [26] Jurado KA, Ariizumi T, Tabata K, et al. Establishment of a lethal mouse model of emerging tick-borne orthonairovirus infections. *PLOS Pathog.* 2024;20(3):e1012101. doi: [10.1371/journal.ppat.1012101](https://doi.org/10.1371/journal.ppat.1012101)
- [27] Bereczky S, Lindegren G, Karlberg H, et al. Crimean-Congo hemorrhagic fever virus infection is lethal for adult type I interferon receptor-knockout mice. *J Gen Virol.* 2010;91(Pt 6):1473–1477. doi: [10.1099/vir.0.019034-0](https://doi.org/10.1099/vir.0.019034-0)
- [28] Zivcec M, Safronetz D, Scott D, et al. Lethal Crimean-Congo hemorrhagic fever virus infection in interferon alpha/beta receptor knockout mice is associated with high viral loads, proinflammatory responses, and coagulopathy. *J Infect Dis.* 2013;207(12):1909–1921. doi: [10.1093/infdis/jit061](https://doi.org/10.1093/infdis/jit061)
- [29] Zivcec M, Spiropoulou CF, Spengler JR. The use of mice lacking type I or both type I and type II interferon responses in research on hemorrhagic fever viruses. Part 2: vaccine efficacy studies. *Antiviral Res.* 2020;174:104702. doi: [10.1016/j.antiviral.2019.104702](https://doi.org/10.1016/j.antiviral.2019.104702)
- [30] Xu Q, Tang Y, Huang G. Innate immune responses in RNA viral infection. *Front Med.* 2021;15(3):333–346. doi: [10.1007/s11684-020-0776-7](https://doi.org/10.1007/s11684-020-0776-7)
- [31] De Santo C, Arscott R, Booth S, et al. Invariant NKT cells modulate the suppressive activity of IL-10-secreting neutrophils differentiated with serum amyloid a. *Nat Immunol.* 2010;11(11):1039–1046. doi: [10.1038/ni.1942](https://doi.org/10.1038/ni.1942)
- [32] Ouyang W, O'Garra A. IL-10 family cytokines IL-10 and IL-22: from basic science to clinical translation. *Immunity.* 2019;50(4):871–891. doi: [10.1016/j.immuni.2019.03.020](https://doi.org/10.1016/j.immuni.2019.03.020)
- [33] Chang EY, Guo B, Doyle SE, et al. Cutting edge: involvement of the type I IFN production and signaling pathway in lipopolysaccharide-induced IL-10

- production. *J Immunol.* **2007**;178(11):6705–6709. doi: [10.4049/jimmunol.178.11.6705](https://doi.org/10.4049/jimmunol.178.11.6705)
- [34] Arimori Y, Nakamura R, Yamada H, et al. Type I interferon limits influenza virus-induced acute lung injury by regulation of excessive inflammation in mice. *Antiviral Res.* **2013**;99(3):230–237. doi: [10.1016/j.antiviral.2013.05.007](https://doi.org/10.1016/j.antiviral.2013.05.007)
- [35] Arshad M, Abdul Hamid N, Chan MC, et al. NUB1 and FAT10 proteins as potential novel biomarkers in cancer: a translational perspective. *Cells.* **2021**;10(9):2176. doi: [10.3390/cells10092176](https://doi.org/10.3390/cells10092176)
- [36] Saxena K, Roverato ND, Reithmann M, et al. FAT10 is phosphorylated by IKK β to inhibit the antiviral type-I interferon response. *Life Sci Alliance.* **2023**;7(1):e202101282. doi: [10.26508/lsa.202101282](https://doi.org/10.26508/lsa.202101282)
- [37] Saxena K, Inholz K, Basler M, et al. FAT10 inhibits TRIM21 to down-regulate antiviral type-I interferon secretion. *Life Sci Alliance.* **2024**;7(9):e202402786. doi: [10.26508/lsa.202402786](https://doi.org/10.26508/lsa.202402786)
- [38] Choi YJ, Bowman JW, Jung JU. A talented duo: IFIT1 and IFIT3 patrol viral RNA caps. *Immunity.* **2018**;48(3):474–476. doi: [10.1016/j.immuni.2018.03.001](https://doi.org/10.1016/j.immuni.2018.03.001)
- [39] Zhu Z, Yang X, Huang C, et al. The interferon-induced protein with tetratricopeptide repeats repress influenza virus infection by inhibiting viral RNA synthesis. *Viruses.* **2023**;15(7):1412. doi: [10.3390/v15071412](https://doi.org/10.3390/v15071412)
- [40] Gizzi AS, Grove TL, Arnold JJ, et al. A naturally occurring antiviral ribonucleotide encoded by the human genome. *Nature.* **2018**;558(7711):610–614. doi: [10.1038/s41586-018-0238-4](https://doi.org/10.1038/s41586-018-0238-4)
- [41] Rabbani MAG, Ribaud M, Guo J-T, et al. Identification of interferon-stimulated gene proteins that inhibit human parainfluenza virus type 3. *J Virol.* **2016**;90(24):11145–11156. doi: [10.1128/jvi.01551-16](https://doi.org/10.1128/jvi.01551-16)
- [42] Du X, Gu H, Sun Y, et al. Ly-6D of Japanese flounder (*Paralichthys olivaceus*) functions as a complement regulator and promotes host clearance of pathogen. *Dev Comp Immunol.* **2021**;122:104104. doi: [10.1016/j.dci.2021.104104](https://doi.org/10.1016/j.dci.2021.104104)